# Split-Ring FSS Spiral Phase Plate

Zelenchuk, D., & Fusco, V. (2013). Split-Ring FSS Spiral Phase Plate. *IEEE Antennas and Wireless Propagation Letters*, *12*, 284-287. https://doi.org/10.1109/LAWP.2013.2247735

**Published in:**
IEEE Antennas and Wireless Propagation Letters

**Document Version:**
Early version, also known as pre-print

Digital Object Identifier: 10.1109/LAWP.2013.224773

# Split Ring FSS Spiral Phase Plate

Dmitry Zelenchuk, *Member, IEEE,* and Vincent Fusco, *Fellow, IEEE*

***Abstract*—This paper gives the first report of a planar phase plate structure based on frequency selective surface, FSS, technology for the generation of helical far-field radiation patterns with circular polarization properties. The unit cell of the structure comprises two orthogonal split ring resonators designed to ensure 180 degrees phase shift between orthogonal transmission coefficients. This property is exploited to obtain progressive rotational phase shift within the structure and thus synthesize 360 degrees spiral phase profile. Measured far-field radiation patterns demonstrate spiral phase front generation for 10 GHz circularly polarized waves transmitted through the structure.**

***Index Terms*—spiral phase plate, beam forming, imaging**

## I. Introduction

Conical beams with helical wavefront find application where faint objects are to be imaged at the periphery of bright objects, with high contrast [1]. Such beams can be generated with non-planar structures such as, the machined spiral dielectric cylinder [2], Fig. 1. In this paper we propose a planar spiral phase plate which uses a quasi periodic FSS whose unit cell elements are orientated to produce a similar wave front transformation as that produced by the well-established 3D spiral phase plate in Fig. 1.

The operating principle of the quasi periodic structure is based on the phase shift obtained by rotation of the element in a unit cell. This method presents a straightforward approach for generation of smooth phase shift avoiding exhaustive parametric studies and dielectric variation requirements pertinent to other design strategies, e.g. [3]. The fundamental paradigm of the rotational phase shift dates back to optical wave plates [4] and waveguide phase shifters [5] and has since been developed for quasi periodic lenses [6] and reflectarrays [7], [8].

Section II of this paper discusses the operation of a conventional spiral phase plate and the phase rotating properties of a double split ring slot FSS. Section III concentrates on the design of a split ring FSS with transmit spiral phase profile. Measurements demonstrating transformation from a circularly polarized (CP) plane wave input to CP conical beam output are given in Section IV.

Manuscript received February 14, 2013.

This work was conducted under the UK Engineering and Physical Science Research council grant EP/G034303/1.

D. Zelenchuk, and V. Fusco are with ECIT Institute, Queen's University Belfast, Belfast, BT3 9DT, UK (e-mail: v.fusco@ecit.qub.ac.uk)

## II. Theory

### A. Spiral Phase Plate

A spiral phase plate can be milled from a solid cylindrical dielectric block of fixed dielectric constant $\varepsilon$ by forming a helix with a step discontinuity, see Fig. 1.

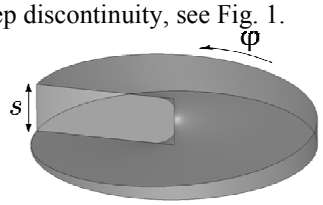


Fig. 1. Dielectric cylinder spiral phase plate.

A plane wavefront of wavelength $\lambda$ passing through the structure is subject to a phase delay, $\psi$, which depends on azimuthal angle, $\varphi$, which in turn is set by thickness $s$ [2],

$$\psi = \frac{(\sqrt{\varepsilon} - 1)s}{\lambda}\varphi$$

After transmission through the structure a null in the centre of the exit beam and linear phase variation with the azimuth appear, i.e. a helical exit wavefront is formed.

### B. FSS phase shifter

Let us assume that a plane wave is normally incident onto the double slot periodic structure with unit cell given in Fig. 2, and that the unit cell can rotate about its origin by angle $\theta_r$. Each slot is resonant to a linearly polarised excitation orthogonal to the split. As a consequence, the slots rotated 90° with respect to each other give rise to resonances that are decoupled. On applying the Jones calculus [4] one can derive the transmitted field through the FSS as

$$\boldsymbol{E}_T = \begin{pmatrix} \cos\theta_r & -\sin\theta_r \\ \sin\theta_r & \cos\theta_r \end{pmatrix} \begin{pmatrix} \mathrm{T}_{x'} & 0 \\ 0 & \mathrm{T}_{y'} \end{pmatrix} \begin{pmatrix} \cos\theta_r & \sin\theta_r \\ -\sin\theta_r & \cos\theta_r \end{pmatrix} \boldsymbol{E}_i$$

where $\boldsymbol{E}_i$ is the incident field vector with $x$ and $y$ components, $\mathrm{T}_{x'}$ and $\mathrm{T}_{y'}$ are the transmission coefficients along the primed coordinates, shown in Fig. 2.

If the FSS is designed to yield $\mathrm{T}_{x'} = -\mathrm{T}_{y'}$ the transmitted field can be expressed as

$$\boldsymbol{E}_T = \mathrm{T}_{x'} \begin{pmatrix} \cos 2\theta_r & \sin 2\theta_r \\ \sin 2\theta_r & -\cos 2\theta_r \end{pmatrix} \boldsymbol{E}_i \qquad (1)$$

For a CP incident wave $\boldsymbol{E}_i = {}^1\!/_2 \begin{pmatrix} 1 \\ \pm j \end{pmatrix}$ it follows from (1) that the transmitted wave should be

$$\boldsymbol{E}_T = \mathrm{T}_{x'} e^{\pm j2\theta_r} \frac{1}{2}\begin{pmatrix} 1 \\ \mp j \end{pmatrix} \quad (2)$$

It follows from (2) that upon passing through the FSS an incident CP wave will change its hand of polarization, will gain a phase shift of $\pm 2\theta_r$, and will experience insertion loss defined by $\mathrm{T}_{x'}$. The sign of the phase shift depends on the hand of the incident wave.

## III. Design

### A. Periodic FSS

The periodic FSS, shown in Fig. 2, is comprised of two aluminium sheets of thickness $t$ separated by air gap of $h$ with split ring slots milled out. A two-layer design is chosen over a single layer one due to almost 1dB better insertion loss [9]. The dimensions of the structure are selected by parametrical analysis to obtain equal amplitude and the 180° phase difference for $x'$- and $y'$- components. Both criteria are enforced by making the slots resonate at frequencies above and below the specified operating frequency of 10 GHz. Since the splits in the slots are rotated 90° with respect to each other, orthogonally polarized excitations give rise to resonances that are decoupled.

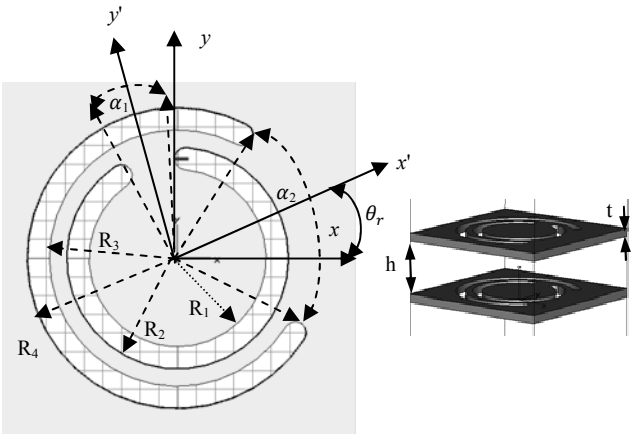


Fig. 2. Double layer FSS structure: (a) top view, (b) cross-sectional view.

TABLE I. PARAMETERS OF THE UNIT CELL

| $R_1$, mm | $R_2$, mm | $R_3$, mm | $R_4$, mm | $\alpha_1$, ° | $\alpha_2$, ° | $h$, mm | t, mm |
|---|---|---|---|---|---|---|---|
| 4.7 | 5.9 | 6.8 | 8 | 21 | 85.6 | 7.5 | 1 |

The simulations were performed with CST Microwave Studio and selected dimensions of the unit cell are given in the Table I. The unit cell is square with period $d = 19$ mm. The study has shown that the FSS response is most sensitive to the slot length variation as it directly affects the resonant frequency, whereas the slot width and the screen thickness have less profound effect on the frequency and mostly affects the bandwidth.

The 10x10 structure with all the elements aligned and no rotation applied was measured to obtain the periodic structure response. Two linearly polarised 15 dB gain horns were placed at 50 cm distance either side of the screen under test, which was surrounded by radar-absorbent material. The horns were connected to a VNA and the $S_{21}$ was measured with and without the FSS to calibrate out the path loss. The edge illumination below -10 dB was maintained and the stray reflections were time-gated from the response.

The simulated and measured characteristics of the FSS are presented in Fig. 3. Here we observe that at the operating frequency the amplitudes of both *y*-directed and *x*-directed components are equal and that the phase difference between them is 180°. Insertion loss measured at 10 GHz is 2.3 dB. Such a level of the insertion loss can be limiting for certain application, however, like for other FSS structures the insertion loss of the structure could, at the expense of thickness, be improved by increasing the number of layers, [6], [10].

The simulated amplitude and phase responses of the structure when illuminated at normal incidence with a CP wave as a function of unit cell rotation are shown in Fig. 4, noting that both upper and lower layers are identically rotated.

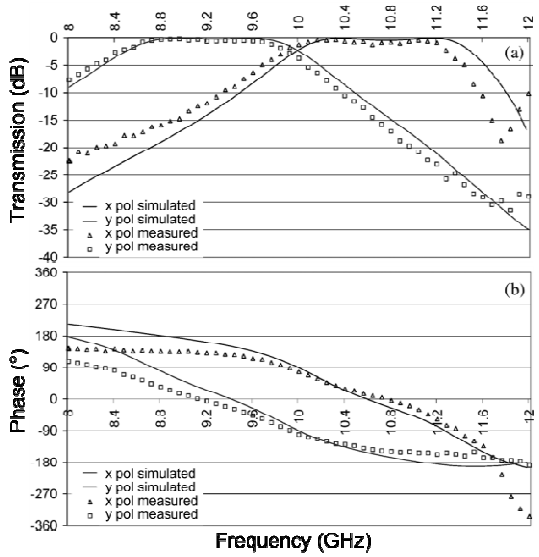


Fig. 3. Unit cell simulated vs measured transmission: (a) amplitude, (b) phase.

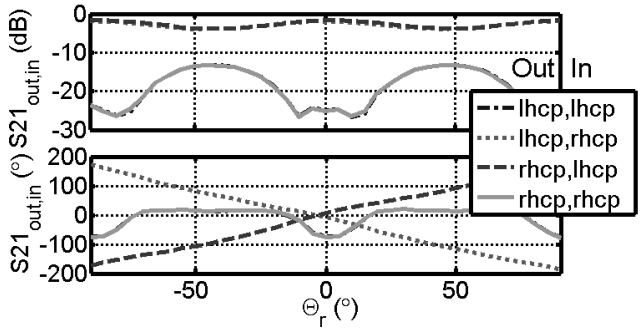


Fig. 4. Simulated transmission amplitude and phase variation with rotation angle $\theta_r$ for normal incidence of CP waves ('out' and 'in' denote polarization of the transmitted and incident waves, respectively).

This study shows that the CP wave passing through the structure gains a phase shift twice that of the rotation angle and that insertion loss varies with rotation angle, from 1.9 dB to 3.9 dB. We also observe that the expected co- to cross-polarization level should be better than 10 dB worst case. Based on the structure above we now study a finite surface

with elements rotated to synthesize a spiral phase distribution.

### *B. Helical wavefront generation with finite split ring FSS structure*

Next we propose a 10x10 element FSS structure with individual elements rotated such that a spiral phase profile can be achieved in order to emulate the phase shifting properties of the 3D dielectric spiral phase plate. The dimensions of each element are as specified in Table I. The spiral phase profile given by (3) is achieved by progressive rotation of each of the 10x10 FSS elements

$$\psi(x,y)=\begin{cases}\tan^{-1}\dfrac{y}{x}, x>0, y>0\\ \tan^{-1}\dfrac{y}{x}+\pi, x<0\\ \tan^{-1}\dfrac{y}{x}+2\pi, x>0, y\le 0\end{cases} \quad (3)$$

Employing (3) at the centres of each unit cell FSS element we present the required resulting phase rotation distribution in Table II. Each element of the plate is then rotated in order to produce the necessary phase shift. The centre of the spiral phase plate is at ($x$=0 mm, $y$=0 mm).

TABLE II. SPIRAL PHASE SHIFT DISTRIBUTION IN DEGREES ACROSS THE SURFACE

| x, mm / y, mm | -85.5 | -66.5 | -47.5 | -28.5 | -9.5 | 9.5 | 28.5 | 47.5 | 66.5 | 85.5 |
|---|---|---|---|---|---|---|---|---|---|---|
| 85.5 | 135 | 127.9 | 119.1 | 108.4 | 96.3 | 83.7 | 71.6 | 60.9 | 52.1 | 45 |
| 66.5 | 142 | 135 | 126 | 113 | 98 | 82 | 67 | 55 | 45 | 38 |
| 47.5 | 151 | 145 | 135 | 121 | 101 | 79 | 59 | 45 | 36 | 29 |
| 28.5 | 162 | 157 | 149 | 135 | 108 | 72 | 45 | 31 | 23 | 18 |
| 9.5 | 174 | 172 | 169 | 162 | 135 | 45 | 18 | 11 | 8 | 6 |
| -9.5 | 186 | 188 | 191 | 198 | 225 | 315 | 342 | 349 | 352 | 354 |
| -28.5 | 198 | 203 | 211 | 225 | 252 | 288 | 315 | 329 | 337 | 342 |
| -47.5 | 209 | 216 | 225 | 239 | 259 | 281 | 301 | 315 | 325 | 331 |
| -66.5 | 218 | 225 | 235 | 247 | 262 | 278 | 293 | 306 | 315 | 322 |
| -85.5 | 225 | 232 | 241 | 252 | 264 | 276 | 288 | 299 | 308 | 315 |

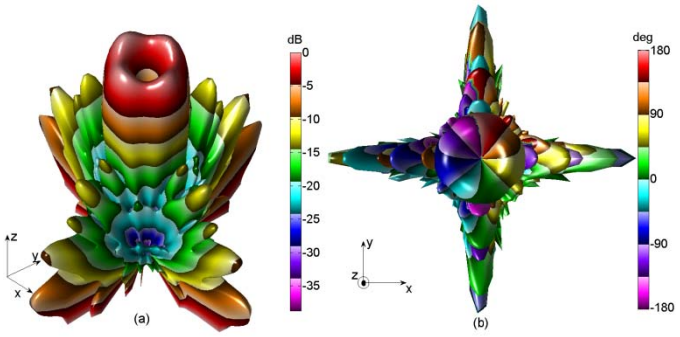


Fig. 5. Predicted array factor of the 10x10 array with spiral phase distribution (a) amplitude, (b) phase.

The far-field exit radiation pattern of the structure upon excitation with a normally incident plane wave can be approximated by, [11],:

$$AF_{\theta,\varphi}=\sum_m\sum_n A_{mn}e^{-j(kx_m\sin\theta\cos\varphi+ky_n\sin\theta\sin\varphi+\psi(x_m,y_n))} \quad (4)$$

where $x_m, y_n$ are the coordinates of the centre of the array element, $\psi(x_m, y_n)$ is phase shift introduced by the element, $A_{mn}$ is the amplitude of the field at the element and $\theta$ and $\varphi$ are the elevation and azimuth of the far-field pattern.

The array factor for the 10x10 array with period of 19 mm and spiral phase distribution shown in Table II at 10 GHz is plotted in Fig. 5. It is evident from Fig. 5 that the far field of the array has the characteristic null in the boresight direction and linear phase variation with azimuthal angle.

### *C. Effect of the phase quantization*

The phase profile of the structure is discrete as shown in Table II, thus the effect of the quantization on the radiation pattern is of interest [12]. The array factor for three structures with the same area but different period and hence number of cells was calculated using (4) and plotted in Fig. 6. It is clear from the plot that shrinking the unit cell size leads to slightly reduced sidelobes levels. However the effect is not significant as the first three peaks are almost identical.

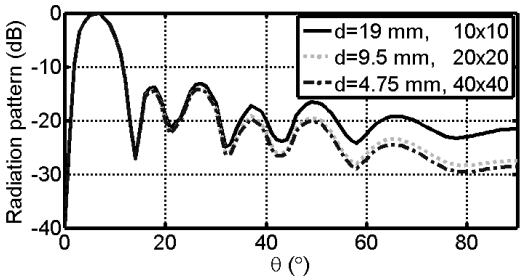


Fig. 6. Simulated radiation patterns xz-plane cuts for different values of $d$ - the period of the unit cell and number of the cells in the FSS.

## IV. MEASUREMENTS

The 10x10 structure with the dimensions given Table I and the elements rotated according to Table II was manufactured and its near field on the exit side of the arrangement measured using an NSI planar near-field scanner. This method of data acquisition allows post processing for 3D far-field radiation pattern generation.

The structure was illuminated by a 20 dB gain dual linearly polarized horn. The FSS was surrounded by absorbing material in order to decouple the incident field and the transmitted field. The experimental setup and device under test are shown in Fig. 7. Measurements were obtained for all four combinations of $x$- and $y$- linear polarizations. The measured transmission matrix was then used to determine the CP response of the structure [6].

As we discussed in the theoretical part of the paper the transformed beam does change the hand of polarization. Hence in the results interpretation below we define the desirable CP beam with helical wavefront as co-polar and the

unwanted pencil beam pattern, despite their relation to the incident wave is opposite.

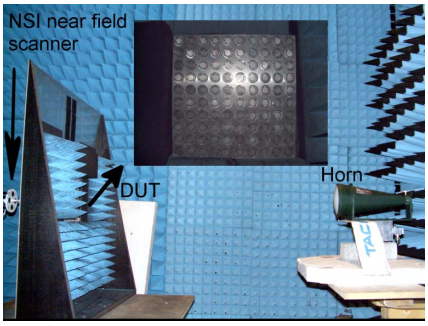


Fig. 7. Experimental setup.

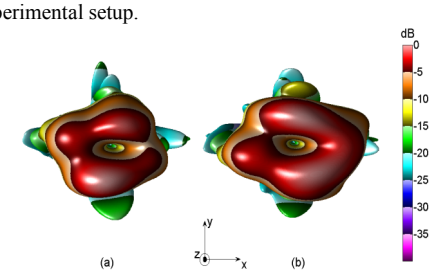


Fig. 8. Measured co-polar CP radiation amplitude pattern (top view): (a) RHCP, (b) LHCP.

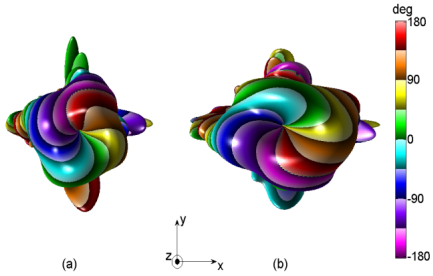


Fig. 9. Measured co-polar phase of CP radiation pattern: (a) RHCP, (b) LHCP.

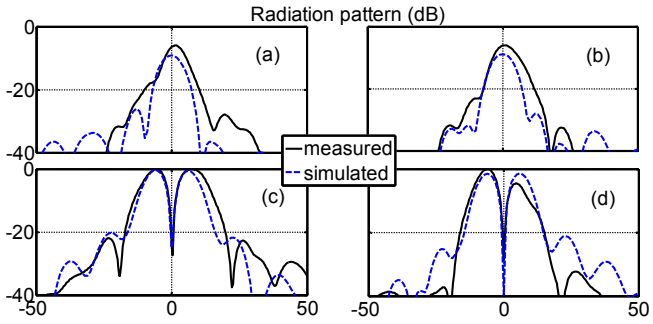


Fig. 10. Measured normalized CP radiation pattern cut in plane $\varphi = 60$ : (a) RHCP (cross-pol), (b) LHCP (cross-pol), (c) RHCP (co-pol), (d) LHCP (co-pol).

The measured amplitude radiation patterns for both right hand CP (RHCP) and left hand CP (LHCP) polarizations at 10 GHz reconstructed from exit near field measurements are given in Fig. 8. The beam structure follows that the one predicted in Fig. 5, i.e. both patterns feature a null in the boresight direction. Moreover when the far-field phase is plotted in Fig. 9, it is apparent that the phase of the main beam exhibits the requisite spiral variation with azimuthal angle.

The freestanding structure was simulated with CST Microwave Studio and bi-static radar cross section upon plane wave excitation was used to compare with measured radiation pattern of the structure, Fig. 10. The measured co-polar CP patterns transmitted through the screen exhibit the expected null at boresight, whereas the cross-polarized CP patterns are pencil-beam like. The measured co-polar central nulls are -29 dB for LHCP and -27 dB for RHCP, c.f. -38 dB and -24 dB simulated, and the cross-polar levels are 6 dB below the co-polar level, c.f. 10 dB simulated. We attribute the higher cross-polar levels to misalignment of the manually rotated elements of the structure with respect to the settings in Table II and the positioning error of the structure itself, Fig. 7.

## V. Conclusion

A new type of planar double layer spiral phase plate was proposed in the paper for the generation of conical beams with CP properties. Based on these properties a planar screen with 360° spiral phase profile was designed and measured. This exhibited helical beam wavefront formation for a normally incident co-polarized CP wavefront and a plane wavefront for the residual cross-polarized field. Such a structure could find application where the CP properties of faint objects are to be imaged at the periphery of bright objects.

## References

[1] G. Foo, D. M. Palacios, and G. A. Swartzlander, Jr., "Optical vortex coronagraph," *Optics Letters*, vol. 30, no. 24, pp. 3308–3310, Dec. 2005.

[2] G. A. Turnbull, D. A. Robertson, G. M. Smith, L. Allen, and M. J. Padgett, "The generation of free-space Laguerre-Gaussian modes at millimetre-wave frequencies by use of a spiral phaseplate," *Optics Communications*, vol. 127, no. 6, pp. 183–188, Jun. 1996.

[3] N. Gagnon, A. Petosa, and D. A. McNamara, "Thin Microwave Quasi-Transparent Phase-Shifting Surface (PSS)," *IEEE Transactions on Antennas and Propagation*, vol. 58, no. 4, pp. 1193–1201, Apr. 2010.

[4] R. C. Jones, "A New Calculus for the Treatment of Optical Systems. I," *Journal of the Optical Society of America*, vol. 31, no. 7, pp. 488–493, Jul. 1941.

[5] A. G. Fox, "An Adjustable Wave-Guide Phase Changer," *Proceedings of the IRE*, vol. 35, no. 12, pp. 1489–1498, Dec. 1947.

[6] R. H. Phillion and M. Okoniewski, "Lenses for Circular Polarization Using Planar Arrays of Rotated Passive Elements," *IEEE Transactions on Antennas and Propagation*, vol. 59, no. 4, pp. 1217–1227, Apr. 2011.

[7] A. E. Martynyuk, J. I. M. Lopez, and N. A. Martynyuk, "Spiraphase-Type Reflectarrays Based on Loaded Ring Slot Resonators," *IEEE Transactions on Antennas and Propagation*, vol. 52, no. 1, pp. 142–153, Jan. 2004.

[8] V. Fusco, "Mechanical beam scanning reflectarray," *IEEE Transactions on Antennas and Propagation*, vol. 53, no. 11, pp. 3842–3844, Nov. 2005.

[9] M. Euler, V. Fusco, R. Cahill, and R. Dickie, "Comparison of frequency-selective screen-based linear to circular split-ring polarisation convertors," *IET Microwaves, Antennas & Propagation*, vol. 4, no. 11, pp. 1764–1772, 2010.

[10] B. A. Munk, *Frequency Selective Surfaces: Theory and Design*. Wiley, 2005.

[11] C. A. Balanis, *Antenna Theory: Analysis and Design*, 2nd ed. John Wiley & Sons, Inc., 1997, p. 960.

[12] H. Nematollahi and J. Laurin, "In-flight reconfigurable reflector antenna based on transmit-array feeding system," in *33rd ESA Antenna Workshop*, 2011, no. October, pp. 1–5.